EFFECTS OF FILM FLOW ON SCALE FORMATION IN HORIZONTAL TUBE FALLING FILM EVAPORATORS FOR SEAWATER DESALINATION

M. Waack[1], *H. Glade[1] and S. Nied[2]
[1] University of Bremen, Engineering Thermodynamics, Badgasteiner Str. 1, 28359 Bremen, Germany,
email: heike.glade@uni-bremen.de
[2] BASF SE, 67056 Ludwigshafen, Germany

ABSTRACT

Horizontal tube falling film evaporators are commonly used in multiple-effect distillation plants for seawater desalination. Steam condenses inside horizontal tubes while seawater flows as a thin film over the outside of the tubes and partly evaporates. The liquid film displays random waves on the surface which affect the transfer rates across the gas/liquid as well as the solid/liquid interface. Thus, scale formation, which is a major problem in falling film evaporators, greatly depends on film flow characteristics. A novel test rig with a high-speed optical micrometer was constructed to study film flow on horizontal tubes. The optical micrometer using LED technology is mounted in a unique way so that the water film thickness can be measured along the tube and around the circumference. Film thickness data at high sampling frequency provide information on wave structure and frequency at different wetting rates. Furthermore, scale formation was studied in a horizontal tube falling film evaporator test rig at pilot plant scale. Artificial seawater was used and different wetting rates were applied in order to systematically investigate scale formation of calcium- and magnesium-containing salts. New insights into film thickness and wave structure of falling liquid films over horizontal tubes and the effects on scale layer characteristics at different wetting rates will be presented and discussed.

INTRODUCTION

In horizontal tube falling film evaporators, which are commonly used in multiple-effect distillation (MED) plants for seawater desalination, crystallization fouling and heat transfer are massively influenced by film flow characteristics on the evaporator tubes. Seawater is distributed by spray nozzles on the upper tube rows of a horizontal tube bundle. The liquid forms a thin film on the outside of the tubes and trickles down tube by tube. The liquid load can be characterized by the wetting rate Γ. It can be defined as the falling film mass flow rate on one side or on both sides of the horizontal tube per unit tube length. In the following, the wetting rate is expressed as the mass flow rate on both sides of the tube per unit tube length:

$$\Gamma = \frac{\dot{m}}{L}. \qquad (1)$$

The film Reynolds number is a common parameter for describing the falling film flow. Different definitions of the film Reynolds number can be found in literature. In the following, the film Reynolds number given by

$$Re_{\mathrm{F}} = \frac{2\,\Gamma}{\eta} \qquad (2)$$

is used with the wetting rate as defined in Eq. (1). In falling film evaporators for seawater desalination, the initial wetting rate on the first tube row commonly ranges between 0.06 kg/s m and 0.14 kg/s m, which corresponds to a film Reynolds number between 250 and 600 for a seawater temperature of 65 °C and a salinity of 35 g/kg. The tubes are heated from the inside by heating steam. As the seawater flows down the tube bundle, it is firstly preheated and subsequently partly evaporates, decreasing the wetting rate far below the initial values.

Seawater is a multi-component salt solution, containing inversely soluble salts, such as calcium carbonate, calcium sulphate and magnesium hydroxide. As the seawater is heated, the solubility of these salts decreases and the supersaturation, the driving force of crystallization, increases. Precipitation of supersaturated salts, mostly calcium carbonate and magnesium hydroxide, preferably starts on the heat transfer surface, forming a scale layer which deteriorates the heat transfer performance. Thus, scale formation needs to be controlled in falling film evaporators to ensure a stable and efficient operation.

Crystallization is driven by supersaturation and it is massively influenced by reaction rates and by mass transfer rates of the involved species towards the heat transfer surface. Mass transfer, in turn, is strongly connected to fluid dynamics. Different flow regimes on and between the horizontal tubes can be identified for different wetting rates.

The intertube flow is characterized by the formation of droplets, jets or sheets on the bottom of each tube [1]. Besides the flow rate, tube spacing, gravity and the physical properties of the liquid determine the flow regime [1]. Droplet formation occurs at low flow rates and large tube spacings. As the flow rate increases or the tube spacing decreases, the flow configuration changes from droplets to jets and finally reaches the sheet regime with respective transition regions in between. Droplets and jets are

ISBN: 978-0-9984188-1-0; Published online www.heatexchanger-fouling.com

mostly present at common film Reynolds numbers in practical applications. The free surface of the liquid exhibits a wave pattern which can be described by Taylor instability theory [2]. On the tube bottom, droplets/jets detach from locations with maximum wave amplitude [2]. The distance between droplet/jet formation sites decreases with increasing film Reynolds number [3]. In the droplet regime, detachment sites are not simultaneously active at first. With increasing film Reynolds number, more droplets detach at the same time and the droplet frequency increases until continuous jets are formed [4]. In the jet regime with low film Reynolds numbers, jet impingement and detachment sites are inline. As the flow rate increases, two impinging jets form a crest in between each other, resulting in a detachment site right underneath [2].

Film flow regimes on tubes can be described by the physical properties of the liquid, the flow rate and the slope of the substrate [5]. The description is complicated due to the presence of the free surface. Below a critical film Reynolds number, the film is mainly laminar. The free surface is covered with capillary and/or gravity waves as the flow rate increases, referred to as wavy laminar regime. The nature of the waves is mainly dependent on the physical properties of the liquid [5]. Finally, the flow is turbulent above a critical film Reynolds number. No matter which flow regime is present, a substantial part of the film is still occupied by a relatively large non-turbulent sublayer [6]. The laminar wavy regime sets in at a film Reynolds number of 20 for film flow on an inclined plate [7]. The transition to turbulent flow has been reported to occur at a film Reynolds number of 2000 on a large-diameter horizontal tube [8]. On horizontal tubes, film flow is additionally influenced by impinging and detaching droplets/jets. The tube perimeter may be divided in an impingement region and a hydrodynamically fully developed region [9]. The above mentioned flow regimes are of concern in the fully developed region. Droplet/jet impingement significantly determines heat and mass transfer rates in the impingement region. Moreover, the film is agitated by the splashing, inducing surface waves which are independent of capillary and gravity waves.

Several studies of film flow on horizontal tubes have been performed [10-13]. The film flow on horizontal tubes has mainly been investigated for sheet and jet regions. Film thickness data are commonly evaluated only in regard to film thickness distributions around the tube. Film flow at circumferential angles of 0° (upper crown line) and 180° (lower crown line) as well as axial variations of film thickness have rarely been examined.

Several methods of measuring the liquid film thickness have been reported in literature [11-13]. Zhang et al. [14] used an optical shadow method, similar to the one in this study, to measure the liquid film thickness on a vertical tube.

The effects of film flow on crystallization fouling in falling film evaporators for seawater desalination have rarely been investigated. Stärk et al. [15] studied scale formation in a falling film evaporator at different wetting rates. Scale layer thickness and scale mass per unit tube surface area decreased with increasing wetting rate. Mabrouk et al. [16] developed a numerical model of a falling film evaporator and showed the effect of an uneven seawater distribution on scale formation.

The objective of this study is to give new insights into the effects of film flow on scale formation in falling film evaporators for seawater desalination.

EXPERIMENTAL

Experiments were performed in two different test rigs in order to investigate film flow characteristics on horizontal tubes as well as their influence on scale formation.

Film flow measurements

Test rig. A unique test rig was constructed for the investigation of the film flow on horizontal tubes, comprising a bank of three tubes and a high-speed optical micrometer, as shown in Fig. 1. A centrifugal pump conveys the test liquid from a supply tank to the test section. The liquid flows through a heating coil, which is placed in a thermostat, in order to adjust the temperature. The volume flow rate is controlled by a needle valve and measured with a turbine flow meter (FCH-midi-PVDF, Biotech, Germany). The flow meter exhibits a measurement accuracy of ±2%. The liquid is distributed onto a bank of 3 tubes. The wetted length of the tubes is 300 mm and the distance between the centers of the tubes amounts to 62 mm. In order to achieve a homogeneous liquid distribution, a perforated transparent polymer tube serves as liquid distribution system. The tube has an outer diameter of 16 mm and a wall thickness of 2 mm. Holes with a diameter of 1 mm are aligned with a distance of 5 mm on the bottom of the tube. The distribution tube is positioned 30 mm above the bank of test tubes. The first two tubes of the test section serve to further homogenize the liquid flow.

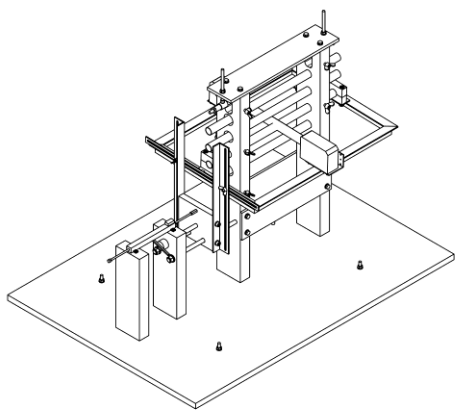

Fig. 1. Film flow test rig.

ISBN: 978-0-9984188-1-0; Published online www.heatexchanger-fouling.com

The liquid film thickness is measured on the third tube by means of a high-speed optical micrometer (optoCONTROL 2600, Micro-Epsilon, Germany) at a high sampling rate. The micrometer uses LED technology and exhibits a resolution of 0.1 µm, a reproducibility of ±1 µm and a linearity of ±3 µm. A light sheet is emitted and directed towards a sensor. The test tube is placed in the light sheet, partially shading the sensor. The shaded length is measured, whereas it is set to zero on the dry tube before each experiment. Once a liquid film is established, the sensor records the film thickness. The optical micrometer is mounted on a steel frame, which in turn is directly fixed on the test tube, avoiding the measurement of vibrations and thermal expansion. The frame can be moved in axial direction of the tube as well as around the tube. The axial position is recorded by means of a potentiometric position sensor (FWA150T, Ahlborn, Germany). The inclination angle is adjusted with a digital protractor.

Test procedure. Film flow experiments were performed with deionized water at a temperature of 25 °C. Aluminum brass tubes (CW 702 R) with an outer diameter of 25 mm and a wall thickness of 1 mm were used. The tube material as well as the dimensions are widely used in MED plants. The test tubes were thoroughly cleaned with isopropyl alcohol and acetone before each experiment. The film thickness was measured along an axial length of 90 mm on the top and bottom of the third tube, referred to as 0° and 180°, respectively. Measurements were performed 45 mm left and right from the center of the wetted tube length in intervals of 5 mm. The center of the wetted tube length is located at a position of 150 mm. Moreover, the film thickness was measured at circumferential angles between 0° and 180° at three different axial positions, namely the center of the wetted tube length as well as 20 mm left and right from the center. Measurements could only be performed from 0° to 50° as well as from 130° to 140° as the light sheet is blocked by the other test tubes at high tilting angles of the steel frame and by pendant liquid on the tube bottom at high circumferential angles. Five different wetting rates were applied, as listed in Table 1. In falling film evaporators, wetting rates can easily fall below the initial value due to evaporation and liquid maldistributions. Therefore, a minimum value of 0.02 kg/s m was chosen. The maximum wetting rate amounted to a common value of 0.10 kg/s m.

Table 1. Investigated wetting rates and film Reynolds numbers for water at 25 °C

Γ	kg/s m	0.02	0.04	0.06	0.08	0.10
Re_F	-	44.9	89.9	134.8	179.8	224.7

Droplet formation is expected to occur for wetting rates below 0.06 kg/s m and jets are expected to form above this value [17]. For each measuring point, the film thickness was recorded for 5 min at a sampling frequency of 230 Hz.

Test evaluation. Film thickness data were processed in order to determine characteristic film parameters. Owing to the dynamic nature of the liquid film, a wide range of film thicknesses was recorded for each measurement. Therefore, statistical evaluation of the data was necessary. The mean film thickness and the average minimum film thickness were calculated.

The surface of the falling liquid film is in wavy motion. In order to analyze the wave motion, the power spectrum was estimated by means of the Welch's method [18]. The power spectrum was calculated by dividing the data into overlapping segments, computing a modified periodogram for each segment and averaging the periodograms. Segments consist out of 600 data points, whereby 400 values are overlapping from segment to segment. In order to increase the resolution in the frequency-domain, zero padding was used and 3600 additional zeros were added to the end of the time-domain signal. Blackman window was chosen as window function. Peaks in the power spectrum can be attributed to harmonic waves, whereby the peak value represents an estimate of the root mean square value of the amplitude at a specific frequency. The highest peak is related to the maximum amplitude at the dominant frequency.

Scaling experiments

Test rig. Scaling experiments were performed in a falling film evaporator test rig at pilot plant scale. Seawater is distributed by an overflow weir onto a bank of 6 horizontal tubes. The tubes are heated by heating steam from the inside, which is generated by a steam generator. The seawater forms a thin film on the outside of the tubes, trickling down from tube to tube. The seawater is preheated on part of the first tube and then partially evaporates on the subsequent tubes. The generated vapor is directed to a plate heat exchanger, where it condenses. The condensate is mixed with the concentrated brine in a surge tank in order to keep the salinity of the seawater approximately constant. The seawater is directed from the surge tank to the top of the evaporator. The temperature inside the evaporator shell is controlled by adjusting the pressure to the respective saturation value by means of a vacuum pump. Various temperature, pressure and level sensors are implemented in the test rig in order to control and monitor the process conditions.

Test procedure. Artificial seawater with a high salinity of 65 g/kg and an ionic strength of 1.39 mol/kg was used for the scaling experiments, representing concentrated brine at the bottom of an MED tube bundle. The initial pH value was approximately 8.3. The formulation of the artificial seawater originates from oceanography, including 99 mass% of salts in natural seawater [19]. An evaporation temperature of 65 °C in the evaporator shell and a condensation temperature of 70 °C inside the tubes were chosen, representing common conditions in the first stage of an MED plant. Due to practical relevance, aluminum brass tubes (CW 702 R) with an outer diameter of

25 mm and a wall thickness of 1 mm were applied and wetting rates ranging from 0.02 kg/s m to 0.10 kg/s m were chosen, as listed in Table 2. Droplet formation is expected at wetting rates below 0.06 kg/s m and jet formation at higher wetting rates [17].

Table 2. Investigated wetting rates and film Reynolds numbers for seawater with a salinity of 65 g/kg at 65 °C

Γ	kg/s m	0.02	0.04	0.06	0.08	0.10
Re_F	-	78.5	157.1	235.6	314.1	392.7

The effective length of the tubes amounted to 453 mm. New tubes were used for each experiment, which were thoroughly cleaned with deionized water, isopropyl alcohol and acetone. Experiments with 240 liters of artificial seawater and time periods of 50 hours were found to be favorable because time periods are long enough to find differences in scale formation and supersaturation levels are still high enough.

Test evaluation. The scaling experiments were evaluated in regard to local scale layer thickness along and around the test tubes as well as calcium and magnesium scale contents.

The scale layer thickness was measured by means of a gauge (MiniTest 2100, ElektroPhysik, Germany) in combination with the probe FN 1.6 using the eddy current method. The measuring range of the probe is between 0 µm and 1600 µm and has a high resolution of 0.1 µm. The tolerance amounts to ±1 µm due to the calibration standard. A two-point calibration was performed for each tube. First, the probe was placed on a clean sample, determining the lower reference value. Afterwards, a calibration foil with a thickness of 96 µm (± 1 µm) was used. The scale layer thickness was measured at four different circumferential angles, namely 0°, 90°, 180° and 270° of the test tube. At each circumferential angle, the scale layer thickness was measured at 25 different points along the tube. The measurements were repeated 10 times at each position.

The scale on the fourth tube was dissolved in hot 0.1 vol.% acetic acid and the concentrations of Ca^{2+} and Mg^{2+} ions in the solution were measured using inductively coupled plasma atomic emission spectroscopy (ICP-AES). The scale layers at both edges (1 cm each) were removed with sandpaper before analysis in order to only determine the scale on the main tube body.

RESULTS

In the following, the results of film flow measurements and scaling experiments are presented. The effects of different wetting rates on film flow characteristics and, thus, on scale formation during falling film evaporation for seawater desalination are under examination.

Film flow on horizontal tubes

Film thicknesses were measured at the top (0°) and at the bottom (180°) of the test tube as well as at different circumferential angles for five different wetting rates. The mean film thickness at each measuring point is presented in Fig. 2 for the top (0°) of the tube and in Fig. 3 for the bottom (180°) of the tube.

At a circumferential angle of 0°, the mean film thickness ranges from 0.109 mm for a wetting rate of 0.02 kg/s m to 0.729 mm for a wetting rate of 0.10 kg/s m. Generally, the mean film thickness along the tube tends to increase with increasing wetting rate. Changes in mean film thickness along the tube are very small for low wetting rates and massively increase for higher wetting rates. Significant variations in mean film thickness along the tube occur for wetting rates of 0.08 kg/s m and 0.10 kg/s m.

At a circumferential angle of 180°, the mean film thickness is about an order of magnitude higher compared to the one at the top (0°) of the tube, as shown in Fig. 3. The mean film thickness along the tube increases with increasing wetting rate. Significant variations in mean film thickness set in for wetting rates of 0.06 kg/s m and above. Changes are rather small for wetting rates below this value.

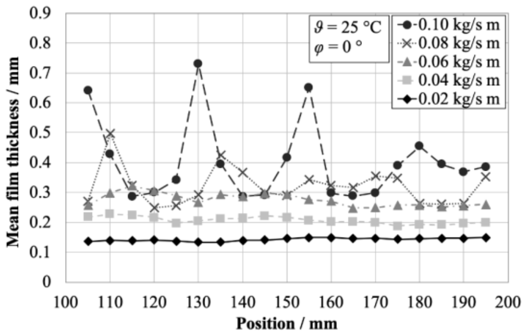

Fig. 2. Mean film thickness along the test tube for different wetting rates at the top (0°) of the test tube.

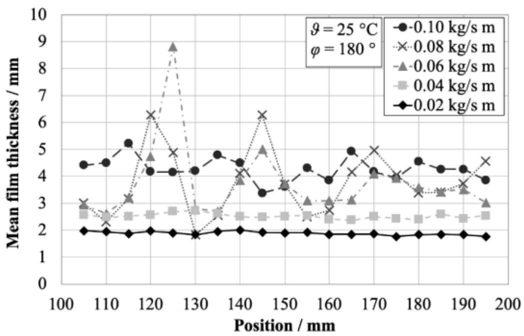

Fig. 3. Mean film thickness along the test tube for different wetting rates at the bottom (180°) of the test tube.

Fig. 4 shows the mean film thickness at different circumferential angles between 0° and 180°. The values represent the average values of the three axial positions 130 mm, 150 mm and 170 mm. The mean film thickness at circumferential angles between 0° and 180° is even lower compared to that at the tube top. It seems to be relatively constant on the upper half of the tube and increases on the lower half of the tube. As already stated for the top and bottom of the tube, the

ISBN: 978-0-9984188-1-0; Published online www.heatexchanger-fouling.com

mean film thickness increases with increasing wetting rate.

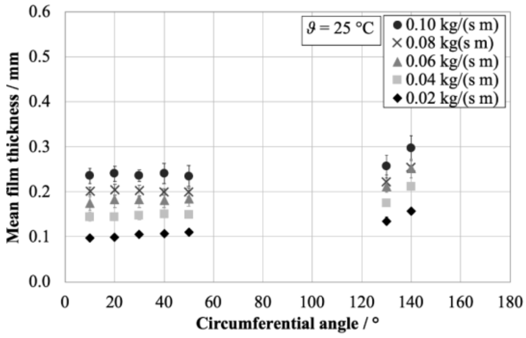

Fig. 4. Mean film thickness at different circumferential angles for different wetting rates. The symbols represent the average of three axial positions (130 mm, 150 mm, 170 mm).

Another parameter of interest is the minimum film thickness. The average values with their standard mean deviation are illustrated in Fig. 5 for the circumferential angles 0° and 180° and in Fig. 6 for circumferential angles in between.

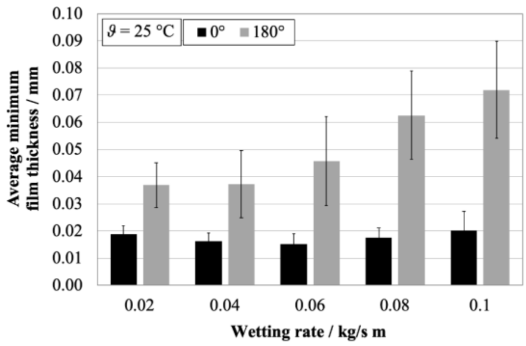

Fig. 5. Average minimum film thickness for different wetting rates at the top (0°) and the bottom (180°) of the test tube.

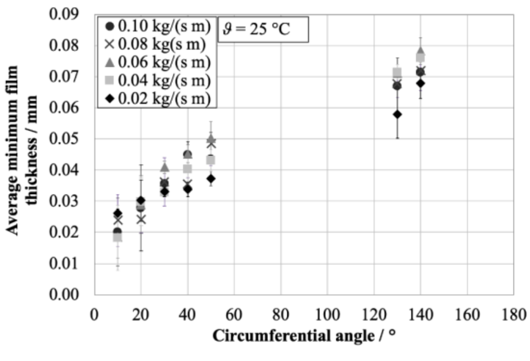

Fig. 6. Average minimum film thickness at different circumferential angles for different wetting rates. The symbols represent the average of three axial positions (130 mm, 150 mm, 170 mm).

At a circumferential angle of 0°, the average minimum film thickness is around 0.017 mm for all wetting rates, as shown in Fig. 5. The average minimum film thickness does not notably change with increasing wetting rate.

At a circumferential angle of 180°, the average minimum film thickness increases with increasing wetting rate, as depicted in Fig. 5. It amounts to about 0.037 mm for a wetting rate of 0.02 kg/s m and it is about 0.072 mm for a wetting rate of 0.10 kg/s m.

The average minimum film thickness increases with increasing circumferential angle. There is no apparent influence of the wetting rate on the minimum film thickness for circumferential angles between 0° and 180°.

In addition to the film thickness data, power spectrum analysis gives further insights into the wave structure of the falling liquid films. The maximum amplitude can be estimated from the power spectrum as well as the dominant frequency of the isolated wave motion. The maximum amplitudes along the tube are illustrated in Fig. 7 for the top (0°) of the tube and in Fig. 8 for the bottom (180°) of the tube. The results for circumferential angles between 0° and 180° are not presented because wave motion behaves similarly to that on the tube top.

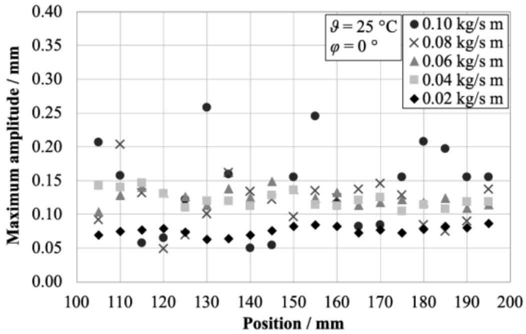

Fig. 7. Maximum amplitude of wave motion on the falling film along the tube for different wetting rates at the top (0°) of the test tube.

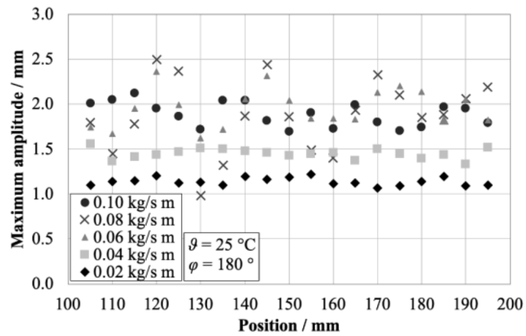

Fig. 8. Maximum amplitude of wave motion on the falling film along the tube for different wetting rates at the bottom (180°) of the test tube.

At a circumferential angle of 0°, the maximum amplitude along the tube increases with increasing wetting rate, as shown in Fig. 7. Minor variations in the maximum amplitude along the tube appear for wetting rates of 0.06 kg/s m and below. However, the maximum amplitude strongly fluctuates at higher wetting rates.

At a circumferential angle of 180°, the fluctuation of the maximum amplitude along the tube already sets in at a wetting rate of 0.06 kg/s m, as depicted in Fig. 8. Compared to the top of the tube, wave amplitudes are much higher. For both circumferential angles, the maximum amplitude correlates very well with the mean film thickness, i.e. a higher mean film thickness results in higher wave amplitudes.

The dominant frequency of the surface wave corresponding to the maximum amplitude along the tube is illustrated in Fig. 9 and Fig. 10 for the two circumferential angles of 0° and 180°, respectively.

For the top of the tube (0°), the dominant wave frequency increases with increasing wetting rate, as shown in Fig. 9. However, significant drops of the dominant frequency along the tube have been determined for wetting rates above 0.06 kg/s m.

In contrast, the dominant frequency of the surface wave with the maximum amplitude at the bottom (180°) of the tube is more or less independent of the wetting rate, as shown in Fig. 10. In general, the dominant frequency at the bottom of the tube is much smaller compared to that at the top of the tube.

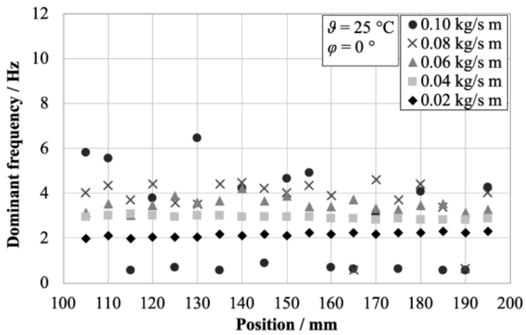

Fig. 9. Dominant frequency of the surface wave with maximum amplitude along the tube for different wetting rates at the top (0°) of the test tube.

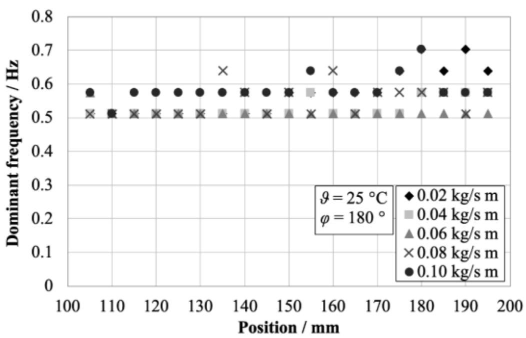

Fig. 10. Dominant frequency of the surface wave with maximum amplitude along the tube for different wetting rates at the bottom (180°) of the test tube.

Scale formation in falling film evaporation

Scaling experiments were performed in the horizontal tube falling film evaporator at five different wetting rates. The masses of calcium and magnesium in the scale layer on the main tube body per unit tube surface area are illustrated in Fig. 11. The main tube body comprises the tube surface excluding the surface corresponding to 1 cm of length at each edge. A small amount of a magnesium salt precipitated on the tube surface, which seems to be unaffected by the wetting rate. The calcium scale content decreases with increasing wetting rate.

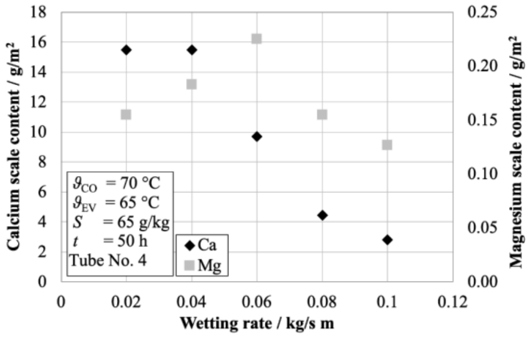

Fig. 11. Calcium and magnesium contents of the scale on the main tube body of the test tube depending on the wetting rate.

The average scale layer thickness on the main body of each tube is presented in Fig. 12 for different wetting rates. The scale layer thickness on each tube decreases with increasing wetting rate, confirming the results of ICP-AES in Fig. 11. In most cases scale formation increases from the top tube (tube No. 1) to the bottom tube (tube No. 6), except for the scale layer thickness at a wetting rate of 0.08 kg/s m, which already exhibits high values on the upper test tubes.

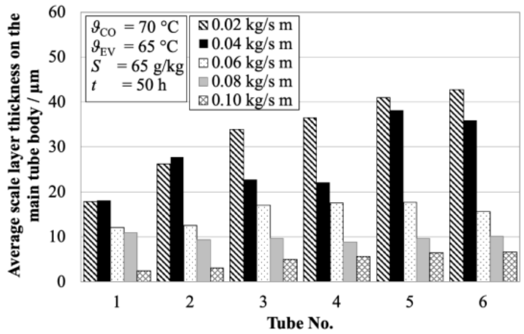

Fig. 12. Average scale layer thickness on the main tube body of each test tube for different wetting rates.

Exemplarily, Fig. 13 shows the average longitudinal scale layer thicknesses on tube No. 3 at the four circumferential angles 0°, 90°, 180° and 270° for the different wetting rates. Scale formation generally decreases with increasing wetting rate at each circumferential angle. However, the scale layer thickness is approximately constant at the bottom (180°) of the tube at low wetting rates. The strongest scale formation occurred at the sides (90° and 270°) of the tube, followed by the tube top. Least scale precipitated at the tube bottom.

ISBN: 978-0-9984188-1-0; Published online www.heatexchanger-fouling.com

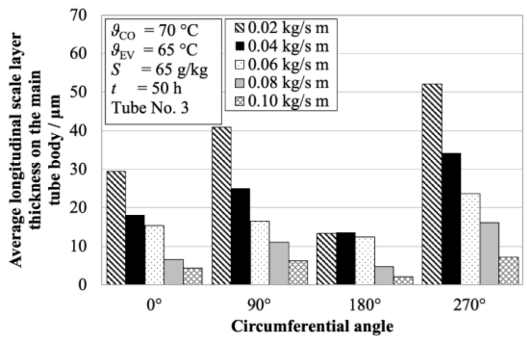

Fig. 13. Average longitudinal scale layer thickness on the main tube body of tube No. 3 at different circumferential angles and wetting rates.

DISCUSSION

Falling film flow on a horizontal tube was investigated on the top (0°) and the bottom (180°) line of the tube and at different circumferential angles between 0° and 180° at different axial positions. Deionized water was used as test liquid. Only minor or no significant differences between falling film flow characteristics of deionized water and seawater are expected [12, 13].

The mean film thickness increases with increasing wetting rate, which is well known from literature (e.g. [12, 13]). No significant changes in mean film thickness are present along the tube for low wetting rates. The positions of impingement sites on the tube top and detachment sites on the tube bottom seem to be non-static, resulting in a more or less homogeneous film thickness along the tube, which confirms the observation of Killion and Garimella [10]. For higher wetting rates, fluctuations along the tube become significant. A regular pattern of minimum and maximum mean film thicknesses can be observed which is a result of the change of the intertube flow regime to jets. Maximum values indicate the most probable positions of impingement and detachment sites. A crest region between two impinging jets at higher wetting rates, as observed by Chen et al. [13], cannot be confirmed, probably due to the stochastic character of the impingement and detachment sites.

The mean film thickness at the top of the tube is in good agreement with measurements at low circumferential angles of other authors [11-13]. The mean film thickness at the tube bottom is about an order of magnitude higher compared to that on the top. Pendant drops and detaching jets massively increase the average film thickness.

The average minimum film thickness at the top of the tube does not notably change with increasing wetting rate compared to that at the tube bottom, where it slightly increases with increasing wetting rate. The average minimum film thickness increases with increasing circumferential angle. Inertia effects seem to dominate on the top of the tube, whereas capillary effects become more important at the bottom. As a result, liquid accumulates on the bottom, leading to higher film thicknesses.

The wave motion of the falling film was analyzed by calculating the power spectrum. Dominant frequency as well as maximum amplitude increase with increasing wetting rate at the tube top. At the tube bottom, the maximum amplitude increases with the wetting rate, but the dominant frequency remains constant.

Dominant frequencies at the tube top most likely represent droplet impingement frequencies. Drop frequencies were measured by Maron-Moalem et al. [4] and fall in the same range as the dominant frequencies.

The dominant frequency on the tube bottom remains practically constant with changing wetting rate. The distance between droplet detachment sites can be described by Taylor instability in dependence of fluid properties and gravity and corresponds to the most unstable wavelength [20]. As the most unstable wavelength is also unaffected by the wetting rate, the dominant frequency probably corresponds to the most rapidly growing film disturbance. Maximum amplitudes increase with the wetting rate because the film thickness increases as well.

In falling film evaporators for seawater desalination, scale formation commonly comprises calcium carbonate and magnesium hydroxide precipitation [21]. The calcium scale content is massively reduced, when the wetting rate is increased, whereas the magnesium scale content shows no obvious trend. Calcium carbonate crystallization on the heat transfer surface seems to be augmented by lower wetting rates, whereas magnesium hydroxide precipitation is unaffected by hydrodynamics and rather determined by electrochemical effects [21]. This trend is confirmed by scale layer thickness measurements. The scale layer thickness is the lowest at the highest wetting rate. Scale formation usually increases from the top tube to the bottom tube due to an increasing salt concentration and therefore higher supersaturations.

The effects of film flow on scale formation are very complex because heat transfer as well as mass transfer are affected. Scale formation depends on reaction kinetics and mass transfer of participating species towards the surface. Moreover, precipitated salt crystals can be removed by shear forces.

Scale deposition can be either diffusion-controlled or reaction-controlled. Hasson's and Perl's model [22], which assumes calcium carbonate crystallization to be diffusion-controlled, is considered to be most successful [23]. Under this assumption, higher mass transfer rates promote scale formation. Further discussion will be based on the assumption of scale formation being diffusion-controlled. The fully developed film is laminar wavy in the experimental range of film Reynolds numbers [7]. Although the film surface exhibits a wave pattern, a relatively thick laminar sublayer is present [6].

The strongest scale formation occurred at the sides of the tubes (90° and 270°), followed by the tube top.

Least scale formed on the tube bottom. Film thickness measurements revealed that the mean film thickness as well as the average minimum film thickness are smaller at the top of the tube compared to those values at the bottom. Thinner films lead to a smaller mass transfer resistance at the tube top, promoting scale formation. Additionally, impinging droplets and jets agitate the film. Wave frequencies are high and amplitudes are about half of the size of the mean film thickness, further intensifying mass transfer. Moreover, thinner films result in higher heat transfer coefficients and therefore high evaporation rates. As a consequence, the smaller minimum film thickness at the top of the tubes leads to high local supersaturations, augmenting salt precipitation. On the bottom of the tubes, films are thick and the dominant wave motion exhibits a low frequency. Therefore, scale formation is less severe at the tube bottom. The mean film thickness is smaller at the tube sides compared to that at the top and the bottom. However, transfer rates are the highest at the tube top, when film flow is not fully developed [17, 24]. Simultaneously, droplet and jet impingement increase shear forces, leading to higher scale removal rates. Since the strongest scale formation was determined at 90° and 270°, the effect of higher removal rates seems to be dominant on the tube top.

Besides mass transfer, film flow massively influences heat transfer and consequently the temperature profile along and around the evaporator tube. In turn, the saturation limits of salts are significantly determined by the surface temperature. A higher temperature results in higher supersaturations of the inversely soluble salts. The temperature around an evaporator tube increases from 0° to 180° and the local heat transfer coefficient decreases, respectively [17, 24]. However, as the temperature difference between condensing steam and evaporating seawater is small, the temperature changes around the perimeter are also rather small. Regarding the temperature profile, scale formation should be the highest at the tube bottom. However, it seems that the small temperature changes around the tube do not play a dominant role.

CONCLUSION

Film flow in falling film evaporators for seawater desalination plays an important role in scale formation on the heat exchanger tubes. Mass and heat transfer are influenced by film thickness and wave motion of the thin seawater film on the tubes. In order to extend the knowledge of film flow on horizontal tubes and to give new insights into the impact of falling film characteristics on scale formation, extensive investigations of both, film flow and scale formation, were performed under different wetting conditions.

Film thicknesses on the bottom of the tube exceed film thicknesses on the top by an order of magnitude. The thinnest film is formed on the tube sides. The mean film thickness increases with increasing wetting rate. Wave formation on the tube top is dominated by droplet/jet impingement, whereas wave motion due to Taylor instability plays a major role at the tube bottom.

Least scale is formed at the bottom of the tube. The scale formation on the top is stronger than that at the bottom. The highest scale thickness was measured at the tube sides. This trend correlates very well with film thickness measurements. Scale content and scale layer thickness increase with decreasing wetting rate because of an intensified mass transfer due to thinner liquid films and wave motion.

In future work, film thickness measurements will be performed at higher temperatures in order to investigate the influence of liquid properties on film thickness and wave motion.

NOMENCLATURE

L tube length, m
$\dot{m}$ mass flow rate, kg/s
Re_F film Reynolds number, dimensionless
S salinity, g/kg
t time, h
Γ wetting rate, kg/s m
η dynamic viscosity, kg/m s
ϑ temperature, °C
φ circumferential angle, °

Subscript

CO condensation
EV evaporation

REFERENCES

[1] Mitrovic, J., *Flow structures of a liquid film falling on horizontal tubes*, Chemical Engineering and Technology, vol. 28, no. 6, pp. 684-694, 2005.

[2] Hu, X., and Jacobi, A. M., *The intertube falling-film modes: Transition, hysteresis, and effects on heat transfer*, no. ACRCCR-5, Air Conditioning and Refrigeration Center, University of Illinois, 1995.

[3] Hu, X., and Jacobi, A. M., *Departure-site spacing for liquid droplets and jets falling between horizontal circular tubes*, Experimental Thermal and Fluid Science, vol. 16, pp. 322-331, 1998.

[4] Maron-Moalem, D., Sideman, S., and Dukler, A. E., *Dripping characteristics in a horizontal tube film evaporator,* Desalination, vol. 27, pp. 117-127, 1978.

[5] Fulford, G. D., *The flow of liquids in thin films,* Advances in Chemical Engineering, vol. 5, pp. 151-236, 1964.

[6] Brumfield, L. K., and Theoanous, T. G., *On the prediction of heat transfer across turbulent liquid films,* Journal of Heat Transfer, vol. 98, no. 3, pp. 496-502, 1976.

[7] Bird, R. B., Stewart, W. E., and Lightfoot, E. N., *Transport Phenomena*. pp. 42-47, vol. 2, John Wiley & Sons, Inc., New York. 2002.

[8] Rogers, J. T., and Goindi, S. S., *Experimental Laminar Falling Film Heat Transfer Coefficients on a Large Diameter Horizontal Tube*, The Canadian Journal of Chemical Engineering, vol. 67, pp. 560-568, 1989.
[9] Chyu, M.-C., and Bergles, A. E., *An analytical and experimental study of falling-film evaporation on a horizontal tube*, Journal of Heat Transfer, vol. 109, pp. 983-990, 1987.
[10] Killion, J. D., and Garimella, S., *Gravity-driven flow of liquid films and droplets in horizontal tube banks,* International Journal of Refrigeration, vol. 26, pp. 516-526, 2003.
[11] Wang, X., He, M., Fan, H., and Zhang, Y., *Measurement of falling film thickness around a horizontal tube using laser-induced fluorescence technique*, Journal of Physics: Conference Series, vol. 147, 2009.
[12] Hou, H., Bi, Q., Ma, H., and Wu, G., *Distribution characteristics of falling film thickness around a horizontal tube,* Desalination, vol. 285, pp. 393-398, 2012.
[13] Chen, X. D., Shen, S., Wang, Y., Chen, J., and Zhang, J., *Measurement on falling film thickness distribution around horizontal tube with laser-induced fluorescence technology*, International Journal of Heat and Mass Transfer, vol. 89, pp. 707-713, 2015.
[14] Zhang, J. T., Wang, B. X., and Peng, X. F., *Falling liquid film thickness measurement by an optical-electronic method*, Review of Scientific Instruments, vol. 71, no. 4, pp. 1883-1886, 2000.
[15] Stärk, A., Loisel, K., Odiot, K., Feßenbecker, A., Kempter, A., Nied, S., and Glade, H., *Wetting behaviour of different tube materials and its influence on scale formation in multiple-effect distillers*, Desalination and Water Treatment, vol. 55, pp. 2502-2514, 2015.
[16] Mabrouk, A. A., Bourouni, K., Abdulrahim, H. K., Darwish, M., and Sharif, A. O., *Impact of tube bundle arrangement and feed flow pattern on the scale formation in large capacity MED desalination plants*, Desalination, vol. 357, pp. 275-285, 2015.
[17] Mitrovic, J., *Wärmeübergang in Rieselfilmen an waagrechten Rohren*, Fortschrittberichte VDI, vol. 211, no. 3, VDI Verlag, Düsseldorf. 1990.
[18] Welch, P. D., *The use of fast Fourier transform for the estimation of power spectra: A method based on time averaging over short, modified periodograms*, IEEE Transactions on Audio and Electroacoustics, vol. 15, no. 2, pp. 70-73, 1967.
[19] Kester, D. R., Duedall, I. W., Connors, D. N., and Pytkowicz, R. M., *Preparation of artificial seawater,* Limnology and Oceanography, vol. 12, no. 1, pp. 176-179, 1967.
[20] Lienhard, J. H., and Wong, P. T. Y., *The dominant unstable wavelength and minimum heat flux during film boiling on a horizontal cylinder,* Journal of Heat Transfer, vol. 86, no. 2, pp. 220-225, 1964.
[21] Krömer, K., Will, S., Loisel, K., Nied, S., Detering, J., Kempter, A., and Glade, H., *Scale formation and mitigation of mixed salts in horizontal tube falling film evaporators for seawater desalination,* Heat Transfer Engineering, vol. 36, pp. 750-762, 2015.
[22] Hasson, D., and Perl, I., *Scale deposition in a laminar falling-film system,* Desalination, vol. 37, pp. 279-292, 1981.
[23] Sheikholeslami, R., and Watkinson, A. P., *Scaling of plain and externally finned heat exchanger tubes*, Journal of Heat Transfer, vol. 108, pp. 147-152, 1986.
[24] Yang, L., Xu, Z., Zhang, X., and Shen, S., *Characterization of the microscopic mechanics in falling film evaporation outside a horizontal tube*, Desalination and Water Treatment, vol. 55, pp. 3330-3335, 2015.

ISBN: 978-0-9984188-1-0; Published online www.heatexchanger-fouling.com